Int. J. Heat Mass Transfer. Vol. 28, No. 3, pp. 573–587, 1985
Printed in Great Britain

0017–9310/85 $3.00 + 0.00

Effect of natural convection on solidification from above and melting from below of a pure metal

C. GAU and R. VISKANTA
School of Mechanical Engineering, Purdue University, West Lafayette, IN 47907, U.S.A.

(*Received* 6 *February* 1984 *and in final form* 27 *August* 1984)

Abstract—The role of natural convection on the solid–liquid interface motion during melting from above and solidification from below of a pure metal was studied. The measurements of both temperature distributions and temperature fluctuations were used as a qualitative indication of the natural convection flow regimes and structures of melt during phase transformation. The photographs of the solid–liquid interface morphology (after draining the melt from the test cell) revealed complicated time-dependent flow structure in the liquid. The measured (average) and predicted solid–liquid interface positions during solidification from above and of melting from below show reasonably good correspondence.

1. INTRODUCTION

MELTING and solidification of metals is of particular interest in materials processing, solidification of castings, metallurgy and purification of metals. A usual assumption in analyzing solid–liquid phase-change heat transfer problems in metals has been that conduction is the sole mode of heat transfer, because metals have high thermal conductivity [1]. However, it has also been recognized that natural convection in the melt during solidification of metals can affect the rate of solidification, the solid–liquid interface and the solid structure through the distribution of impurities [2–7]. For example, the solidification experiments [2] in a cylindrical column of lead revealed that during downward freezing the heat transfer rates associated with Bénard convection were less under transient than under steady state conditions. It was demonstrated [6] that natural convection affects the shape of a stationary and a transient interface in a rectangular tank with a heat source and sink on the two vertical sidewalls. Natural convection in the melt during solidification of castings also plays an important role in modifying the solid structure [4, 5].

The role of natural convection on the solid–liquid interface motion during melting of a low fusion temperature eutectic (Lipowitz metal) has been studied experimentally [8]. The results showed that both diffusion and buoyancy driven natural convection influence the solid–liquid phase-change process during melting from below and solidification from above, and the two transport mechanisms could not be separated. This inhibited analysis and made it very difficult to interpret the experimental data. In order to study the heat transfer during melting and solidification in this type of system mass transfer has to be well understood *a priori*. Unfortunately, although binary systems during phase transformation are being currently studied, many problems remain unresolved [9]. Additional components present in the system contribute significantly to the difficulties. For example, in a ternary system the phase diagram is not on a plane but on a space. The liquidus and solidus are a surface, and interactions among solute diffusion and convection may occur. In the system previously used, the Lipowitz metal has four different components. The inherent mass transport processes which occur during phase transformation have severely complicated the analysis. In order to separate the effects of species diffusion, segregation and natural convection a pure metal must be used as a test material.

This paper reports on an experimental study of solid–liquid phase change heat transfer in unstable situations when natural convection is present in a pure metal melt. The primary objective of the work was to delineate the importance of thermal convection and to gain improved understanding of the processes. Among many possible candidates for the phase change materials, gallium was selected because it has a melting point ($T_f = 29.78°C$) close to the ambient and is nontoxic as well as chemically inactive with air and water. This has made the design of the test cell and the handling of gallium during the experiments relatively simple. Unfortunately, pure gallium is very expensive and this necessitated the use of a small test cell. The importance of natural convection on the solid–liquid interface motion and on the interface morphology are demonstrated by the temperature fluctuation and distribution measurements as well as by photographs taken of the solid–liquid interface. The average interface positions measured are compared with predictions based on a model which assumes that the interface is plane.

2. EXPERIMENTS

2.1. *Test apparatus and instrumentation*

Solidification and melting experiments were performed in a rectangular test cell (Fig. 1) that had inside dimensions of 8.89 cm in height, 6.35 mm in width, and 3.81 cm in depth. The two horizontal walls, which

NOMENCLATURE

c	specific heat
Fo	Fourier number, $\alpha t/H^2$
g	gravitational acceleration
H	height of the cavity
Δh_f	latent heat of fusion of the phase change material
h	heat transfer coefficient
k	thermal conductivity
k^*	thermal conductivity ratio, k_l/k_s
Nu	Nusselt number, $h(1-\delta)H/k_l$
Pr	Prandtl number, ν/α
Ra	Rayleigh number, $g\beta(T_{wb}-T_f)(H-s)^3/\nu\alpha_l$
Ste_l	Stefan number for melting, $c_l(T_{wb}-T_f)/\Delta h_f$
Ste_s	Stefan number for solidification, $c_s(T_f-T_{wt})/\Delta h_f$
s	solid–liquid interface position
T	temperature
x	horizontal distance from the line of symmetry
y	vertical distance from the top of the cavity
z	horizontal distance normal to the x–y plane.

Greek symbols

α	thermal diffusivity
β	thermal expansion coefficient of liquid
ρ	density
ν	kinematic viscosity
τ	$FoSte$; $\tau_l = FoSte_l$ and $\tau_s = FoSte_s$
θ	dimensionless temperature, $(T-T_{wt})/(T_f-T_{wt})$
δ	dimensionless interface position, s/H.

Subscripts

b	bottom plate
f	fusion point of material
l	liquid state
o	initial state
s	solid state
t	top plate
w	wall.

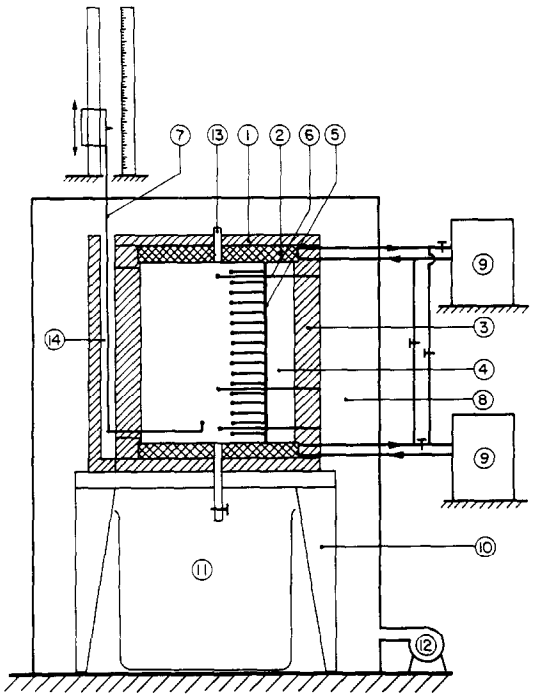

FIG. 1. Schematic diagram of test apparatus: (1) insulation, (2) heat exchanger, (3) Plexiglass wall, (4) phase change material, (5) thermocouple rack, (6) small diameter thermocouples, (7) L-shaped movable probe, (8) temperature controlled environment, (9) constant temperature bath, (10) support frame, (11) container, (12) heat gun with temperature controller, (13) hole for inserting movable probe and (14) vertical slot.

served as the heat source/sink, were made of multipass heat exchanger machined out of copper plate. The copper surfaces were plated with a layer of 0.0127-mm thick chromium for protection against corrosion. All of the vertical walls were made of Plexiglass: the two vertical sidewalls were 1.27-cm thick plates to support the cell; and, for better insulation, the front and back walls had a 0.318-cm air gap between the plates. One of the plates is 0.318-cm thick and the other is 0.635-cm thick.

Five thermocouples were inserted through the copper plates and epoxyed separately into five small diameter holes drilled close to the surface of the copper plates. A vertical slot 0.15 cm in width by 7.62 cm in length was milled in one of the vertical sidewalls for the insertion of an L-shaped probe. Through the vertical slot the liquid metal can be sucked in or expelled by the contraction or expansion of metal during phase transformation. A 0.635-cm diameter hole, drilled through the bottom plate and connected with a tube that is coupled with the vertical slot in the sidewall, serves to drain the liquid and to expose the shape of the solid–liquid interface. To prevent the freezing of the material in the tube at the bottom of the test cell and on the outside of the vertical slot, a long narrow-diameter cable electric heater was immersed and heated.

Eighteen calibrated thermocouples (with a calibrated accuracy of $\pm 0.1°C$) each having a wire diameter of 0.127 mm and sheathed in a 1.27 mm OD stainless steel tube, were equally spaced in the center of the test cell to measure the temperature distributions. The thermocouple rack could be removed when not in

use. To measure the temperature fluctuations when the thermocouple rack was not in use, three additional thermocouples were inserted through three small holes drilled separately on the vertical wall that had no slot. They were located in the central region at 4.67 mm, the second one at 24 mm above, and the third one at 77.79 mm above the bottom plate, respectively. The beads of all the thermocouples were coated with a thin layer of high thermal conductivity epoxy for protection.

The test cell was placed in a transparent box made of Lexan where the temperature could be regulated and kept constant by a temperature controller. The purpose of the controlled environment was to minimize the heat loss/gain between the test cell and the ambient surroundings. A heat storage material was also placed in the box to minimize the frequent on-and-off-switching of the heater and to keep the inside temperature close to a constant value.

2.2. *Experimental procedure and data reduction*

In the experiments, the working material used was gallium. The metal is rather expensive (approx. U.S. \$1 g^{-1}) and is usually used to combine with other pure elements to form electronic and industrial materials such as semiconductors, laser diodes, solar cells and magnetic bubble devices. The pure solid gallium is polycrystalline and the crystals are orthorhombic in structure. The gallium used had purity of 99.6% and melting temperature of 29.78°C. All of the thermophysical properties of gallium are well documented [10] and are summarized in Table 1. However, the thermal conductivity of the solid crystal is highly anisotropic and is 40.82 W m^{-1} K^{-1} along the *a*-axis of the crystal, 88.47 W m^{-1} K^{-1} along the *b*-axis, and 15.99 W m^{-1} K^{-1} along the *c*-axis. The thermal conductivity of liquid gallium is still anisotropic but is not much different along each of the crystal axes.

Before each experiment the solid gallium was melted and poured into the preheated test cell through the sprue on the left side. Provision was made to avoid air bubble entrapment in the test cell. This was accomplished during the filling procedure by a slight lifting of one of the side walls where a small hole had been drilled near the top plate. This hole was sealed after the test cell was filled.

Table 1. Thermophysical properties of gallium

	Solid	Liquid
ρ (kg m^{-3})	5907.0_{20}	$6094.7_{29.8}$
	$5903.7_{29.65}$	$6093.0_{32.4}$
		5972.0_{200}
c (kJ kg^{-1})	0.372	0.398
k (W m °C^{-1})	$33.49_{29.8}$	$33.49_{29.8}$
ν (m^2 s^{-1})		$0.287 \times 10_{30}^{-6}$
h_f (kJ kg^{-1})	80.16	
T_f (°C)	29.78	
β (°C^{-1})		12×10^{-5}
Pr		0.0208_{30}

Numerical subscripts refer to temperature in °C.

The initial temperature inside the test cell was kept uniform, and only a single phase was allowed to exist. This was done by circulating a constant temperature fluid in both heat exchangers at a temperature slightly above or below the fusion point for a sufficient period of time. Melting or solidification was initiated by switching one of the heat exchangers to another constant temperature bath preset at a different temperature. A uniform solid temperature was reached, usually between 1 and 2°C below the fusion temperature of the metal, before melting was initiated. This was done to eliminate subcooling as a parameter of the problem.

Both the pour-out method and the probing method were used to examine and/or measure the shape of solid–liquid interface [8]. In the pour-out method, the liquid was poured out at predetermined times through the sprue or through the tube at the bottom of the cell. The pour-out method was used when the interface shape was non-planar. The liquid was poured out rapidly at preselected times and its volume was measured with a graduated cylinder. The exposed interface was examined, photographed, and the shape near the front and back walls was traced onto transparent paper. The data at succeeding time increments was obtained by performing another experiment with identical boundary and initial conditions.

In the probing method, a Vernier caliper was used to measure the distance an L-shaped probe traversed the liquid. It was inserted in the liquid region through the sprue. This probe allowed for a vertical motion along the vertical slot milled in the side wall between the sprue and the test cell. The measurement error resulting from the deflection of the probe tip during the measuring period was pre-determined and minimized.

3. ANALYSIS

It is well recognized that the solid–liquid interface is non-planar not only because of natural convection in the melt but also because of crystallographic effects of gallium crystals. As a first approximation in estimating the 'average' interface position it is assumed that solidification and melting are one-dimensional. This eliminates the need to solve the complete system of fluid flow and energy equations in the melt, of the energy equation in the solid having an anisotropic thermal conductivity together with the appropriate interface conditions at the moving boundary. This is indeed a very formidable task.

We assume that all of the thermophysical properties, except the density in the buoyancy term, are constant. The rate of melting (freezing) is controlled by the relative magnitude of heat transfer to each side of the solid–liquid interface and the latent heat of fusion absorbed (liberated) at the interface. Lacking a better data base, natural convection heat transfer in the liquid at the interface was modeled by steady heat transfer correlations for cavities without phase change [11].

The nonlinearity introduced by the motion of the solid–liquid interface and natural convection in the liquid precluded a closed form analytical solution of the model equations. Therefore, the integral method used earlier [8] was adopted because of its simplicity. Since the analyses for solidification and melting are practically identical, only the approach for solidification is presented.

In dimensionless form, the energy balance at the interface ($\xi = \delta$) becomes

$$\frac{d\delta}{d\tau} = \frac{\partial\theta_s}{\partial\xi} + k^* \frac{Nu}{(1-\delta)}(\theta_{wb}-1). \quad (1)$$

The energy equation in the solid can be expressed as

$$Ste_s \frac{\partial\theta_s}{\partial\tau} = \frac{\partial^2\theta_s}{\partial\xi^2}. \quad (2)$$

The initial, boundary and interface conditions become, respectively

$$\theta_l = \theta_o \geqslant 1, \quad \delta = 0, \quad \tau \leqslant 0 \text{ during freezing} \quad (3)$$

$$\theta_s = \theta_o \leqslant 1, \quad \delta = 1, \quad \tau \leqslant 0 \text{ during melting} \quad (4)$$

$$\theta_s = 0, \quad \xi = 0 \quad (5)$$

$$\theta_l = \theta_{wb}, \quad \xi = 1 \quad (6)$$

$$\theta_l = \theta_s = 1, \quad \xi = \delta. \quad (7)$$

We assume a second-order polynomial in ξ for the temperature distribution

$$\theta_s = \phi(\tau)(\xi/\delta) + [1-\phi(\tau)](\xi/\delta)^2 \quad (8)$$

which satisfies the temperature boundary conditions. The unknown function $\phi(\tau)$ can be found from

$$2-\phi = [-(b+c)+\sqrt{(b+c)^2+4c}]/2 \quad (9)$$

where

$$b = \left(\frac{\delta}{1-\delta}\right)k^* Nu(\theta_{wb}-1); \quad c = 2/Ste_s. \quad (10)$$

The final form of the differential equation for the solid–liquid interface position becomes

$$\frac{d\delta}{d\tau_s} = \left(\frac{2-\phi}{\delta}\right) + k^* \frac{Nu}{(1-\delta)}(\theta_{wb}-1). \quad (11)$$

Equation (11) was solved numerically for the interface position δ.

4. RESULTS AND DISCUSSION

4.1. *Solidification from above*

Interface shape and flow structure. The interface position and morphology during phase transformation can be controlled by the thermal conditions in the solid and the liquid phases in the vicinity of the interface and by the crystallographic factors. According to the Jackson criterion [12], the solidification is to proceed by lateral growth or faceted growth because of the relatively high entropy of fusion. Thus, the gallium crystal has a preferred growth direction, and the formation of new planes is controlled by two-dimensional nucleation or a screw dislocation mechanism when deformation occurs. The growth rate of gallium crystal can increase rapidly when dislocations or deformations are introduced into the growing crystal [13]. The visual examinations of the solid–liquid interface shape using the pour-out method at preselected times indicated that the shape was irregular and 'corrugated' and had the appearance of regular crystalline structure (Fig. 2). Usually, the region which has a wider and larger facet on the interface has a higher growth rate than the region which has the smaller facet. These are attributed to the combined effect of the growth morphology of freezing front during phase transformation and the highly anisotropic thermal conductivity of the solid crystal.

The interface contour traced along the front and back walls of the test cell at any instant of time appears to be irregular (Fig. 3). The anisotropy in the thermal conductivity and crystallographic effects play a role in controlling the shape of the interface, even very late in the process when natural convection heat transfer in the melt dominates the macroscopic interface shape. In the

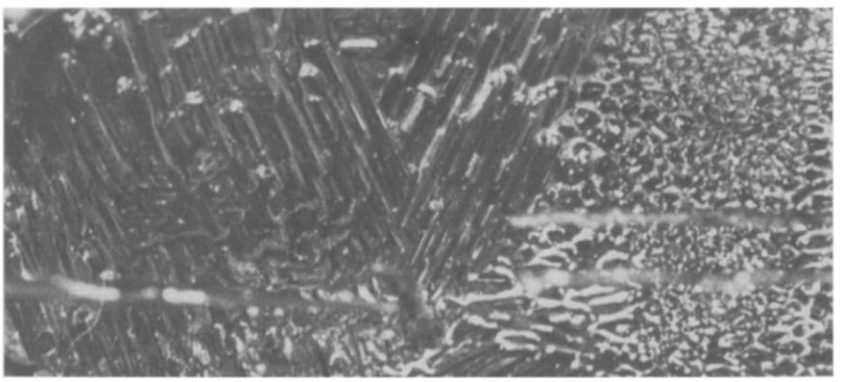

FIG. 2. Typical interface shape during solidification from above at $T_{wt} = 12.3°C$, $T_{wb} = 33.3°C$ and $t = 14$ min (on the right part of the photograph slower solidification rate occurs and smaller facets can be observed).

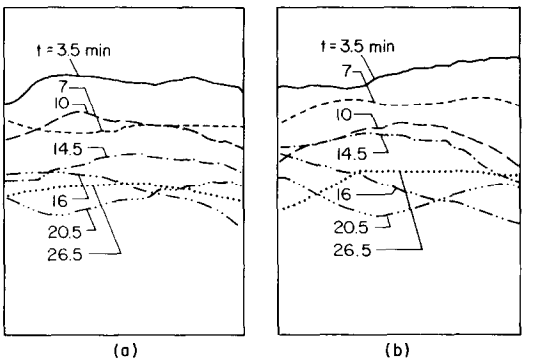

FIG. 3. Interface contour traced along the front wall (a) and the back wall (b) of the test cell during freezing from above, $T_{wt} = 12.3°C$ and $T_{wb} = 33.3°C$.

experiments, the flow structure in the vicinity of the phase-change boundary could not be inferred from the highly irregular interface shape. In some of the experiments, the interface may tilt or become concave as shown in Fig. 3 at $t = 16$ min. The irregular shape and growth morphology of the crystal may also have a significant effect on the flow patterns near the interface. The flow structure, in turn, can modify the interface shape. Because of the complicated mechanisms controlling the solidification process, the interface shape and the flow patterns were not reproducible.

Temperature distributions. Typical vertical temperature distributions measured near the central region at specific times are shown in Fig. 4. In the solid, the temperatures decrease due to the growth of the frozen layer, while in the liquid the temperature distributions

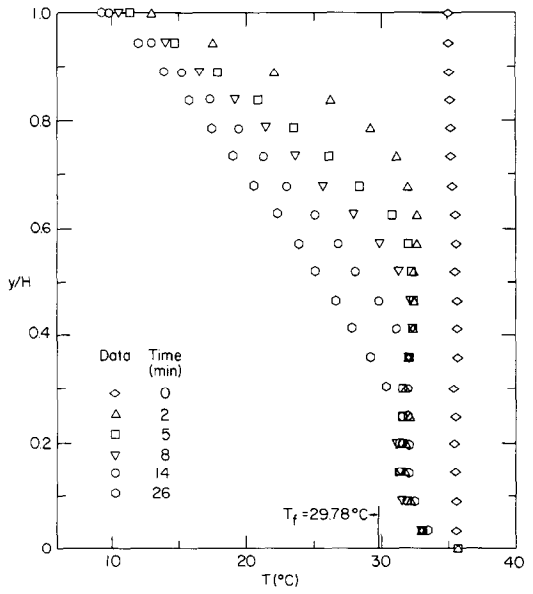

FIG. 4. Vertical temperature distribution measurements in the central region during solidification from above with $T_{wt} = 10.3°C$ and $T_{wb} = 35.6°C$.

are characteristic of natural convection and changed relatively little during the course of the solidification. The temperature gradient in the solid near the interface was initially much greater, then decreased at later times and finally approached the temperature gradient in the liquid near the interface. Therefore, the motion of the solid–liquid interface was expected to decrease and finally terminate when the temperature gradient on both sides of interface were the same.

A slight temperature gradient reversal in the melt layer and a relatively large temperature gradient near the bottom plate can be observed. These are due to the intense natural convection which drives the heated parcels of fluid to the upper region (solid–liquid interface) even when the initial superheating of the melt layer is small (Fig. 4).

Temperature fluctuations. Natural convection is initiated shortly after coolant circulation is started through the top plate. Both the temperatures at 4.76 mm and at 24 mm above the bottom plate in the liquid layer decrease sharply and begin fluctuating (Fig. 5). This was caused by the heavier cooled parcels of fluid passing over the sensor during their descent. After the initially short transient period of oscillation, the temperatures traced at both locations became steady with a nearly constant amplitude and frequency of fluctuations. However, the average amplitude and frequency of temperature fluctuations near the bottom plate were larger than near the central region. As solidification proceeded, the mean temperature near the central region showed only a slight increase until the sensor reached the edge of the thermal boundary layer. The mean temperature started to decrease and the amplitude of the fluctuations increased initially and decreased later. Although presence of convection cells in the liquid layer could not be confirmed from the available temperature measurements, the stable temperature fluctuations and distribution measurements suggest that the bulk flow in the liquid layer may be nearly quasi-steady.

Comparison of measured and predicted interface positions. Both the pour-out method and the probing method were used to obtain the interface position. The experimental data are compared with the predictions in Fig. 6. The data points obtained using the probing method are smooth and agree well with the predictions. The measurement errors due to the irregularity of the interface are not as large compared with the average interface position measured using the pour-out method. All the data points are below the predictions at early times and above the predictions at later times. The slower freezing rate measured at early times may be due to the poor thermal contact between the metal and the top wall of the heat exchanger. Before the solidification was initiated, a thin oxide layer may have floated to the top and decreased heat transfer from the metal to the heat exchanger. The effect of poor thermal contact was gradually reduced as freezing progressed. The

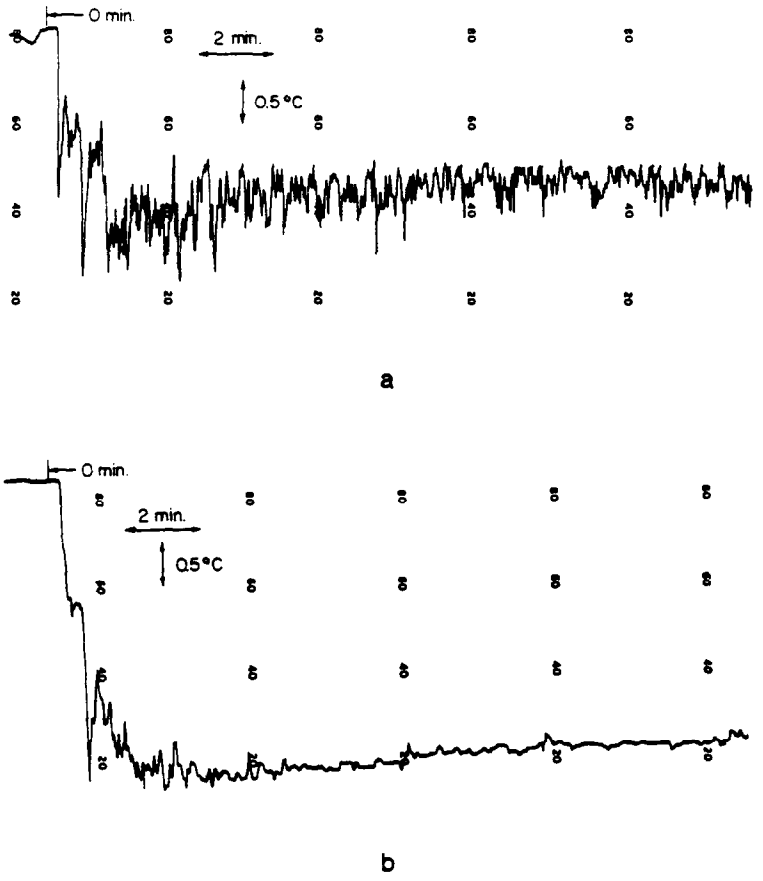

FIG. 5. Temperature fluctuations during freezing from above with $T_{wt} = 12.3°C$ and $T_{wb} = 33.3°C$: (a) for the thermocouple located 4.76 mm above the bottom plate and (b) for the thermocouple located 24 mm above the bottom plate.

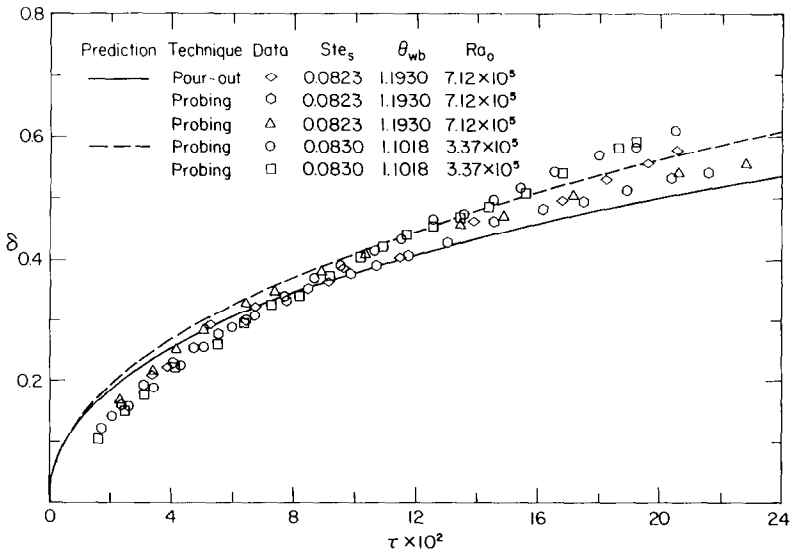

FIG. 6. Comparison of the measured and predicted interface positions during solidification from above.

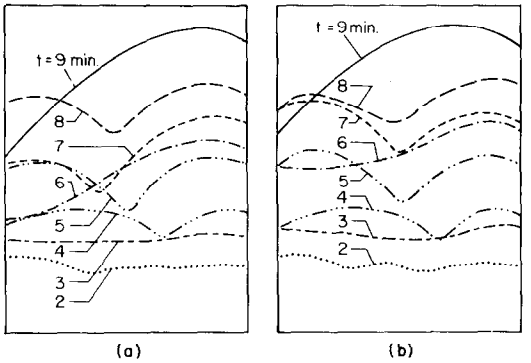

FIG. 7. Interface shape traced along the front wall (a) and the back wall (b) of the test cell during melting from below, $T_{wb} = 46.0°C$.

solidification at later times is primarily controlled by the relatively large thermal resistance in the solid. The higher growth rate measured at later times is attributed to the anisotropic thermal conductivity of gallium crystal. As predicted, natural convection can initially retard and finally terminate the process.

4.2. *Melting from below*

Interface shape and inferred flow structure. During the melting experiments from below, the typical solid–liquid interface shapes traced along the front and the back walls at specific times are shown in Fig. 7. Initially, the solid–liquid interface was flat and natural convection in the melt was absent. Later, the interface shape became irregular and was controlled to a large extent by the buoyancy induced flow in the liquid. Since the average aspect ratio of the liquid changes continuously the results of Fig. 7 clearly show that the side walls or the aspect ratio have a significant effect on the solid–liquid interface shape. The photographs (Fig. 8) show the interface shape at early times for the same thermal conditions as those for the experiment of Fig. 7. Both the hemispherical capped cells with hexagonal edge and the semi-cylindrical capped rolls with their axes perpendicular to the shorter dimension of the test cell were observed for different runs with the same bottom wall temperature (Figs. 8b and 8d). The interface morphology is determined by the different modes of natural convection. Therefore, the flow patterns at early times could be either the Bénard convection cells or cylindrical convection rolls. In some experiments both types of convection modes coexisted in the melt. This can be deduced from the interface shape in Fig. 9d. The right-hand side was formed by the convection rolls while the left-hand side by the Bénard cells. The convection rolls have not been observed during melting of a paraffin and water from below for which the liquid phase has a relatively high Prandtl number [14]. Under the Bénard capped cells the liquid rose in the central region of the cell and fell around the edges of the cell. When the fluid motion was in a form of a convection roll the fluid rose along the front and back walls and fell down near the central region of test cell.

The Bénard cells observed during melting of gallium from below are significantly larger than those observed during melting of paraffin [14] and a complete cell hardly ever occurred. The relatively large size Bénard capped cells (cylindrical capped rolls) observed in a metal are attributed to the late establishment of the convection cells (rolls). Due to the high initial velocity of the solid–liquid interface motion (high temperature gradient and large thermal conductivity across the melt layer and a relatively small latent heat of fusion of the metal) by the time the Bénard cells (or convection rolls) were well established the melt layer had already been relatively thick.

Growth in size and reduction in the number of Bénard cells as the melting proceeded was expected. However, the fact that the edge of Bénard capped cell appeared sharper at later times (Fig. 8b) and that only two quarters of a Bénard cell were left at the final stages of cellular convection (Fig. 8c) indicate the growth and the combination process of the cells.

For experiments with a higher bottom wall temperature, the same conclusions can be drawn except that the size of the complete and of the incomplete Bénard cells are much smaller and the number is larger when the Bénard convection mode had occurred (Fig. 9). The larger number of cells observed initially can be explained by the fact that natural convection is initiated at a smaller aspect ratio for a higher bottom wall temperature.

A series of experiments for a lower bottom plate temperature during melting have also been performed [15]. Only two convection rolls have been observed. It was found that the axes of the convection rolls were always perpendicular to the shorter dimension of the test section. This is different from the findings for laminar natural convection in a box during heating from below of a relatively high Prandtl number fluid ($Pr > 0.71$) [16]. Because of the low Prandtl number of the liquid metal ($Pr = 1$), sidewalls did not have any effect on the shape of the convection rolls. The convection rolls also grew in size as the melt layer increased in depth. However, the number of convection rolls persisted only until the flow became unstable.

The convection rolls (cells) may become distorted and finally break up as the melting proceeds. During the transition period from laminar to turbulent ('random laminar') flow the complicated flow pattern due to the break up of the cells or rolls made the interface irregular. The irregular interface has been observed and can be inferred from the interface shape at the front and the back walls in Fig. 7. At later times, the solid–liquid interface exhibited mostly a concave shape to the solid in the x-direction and was flat or sometimes slightly wavy in the z-direction. The observations suggest that the axis of the circulating flow is perpendicular to the front and the back walls (Fig. 7). The fluid rose along one of the vertical sidewalls and fell along the other sidewall where a slower melting rate can be observed. The direction of the circulating motion can thus be inferred but may not be the same for different

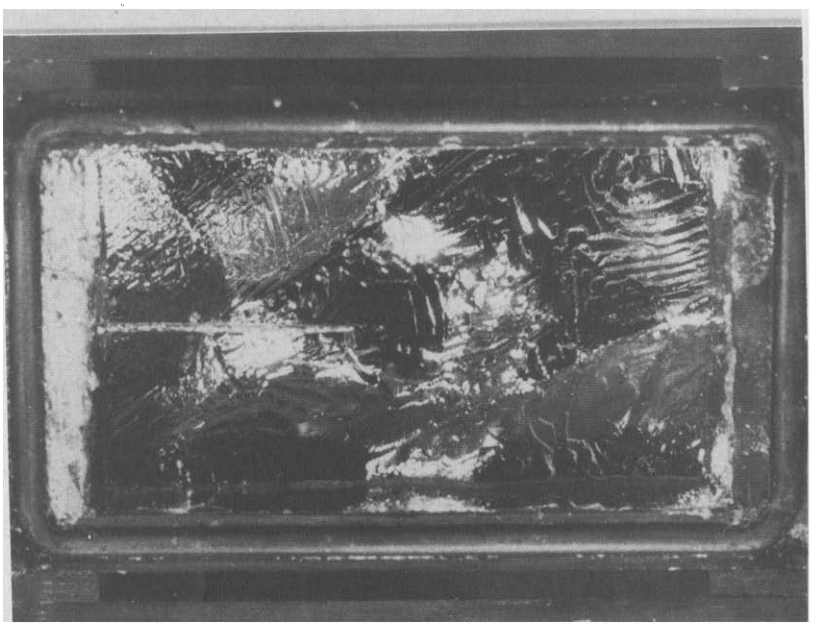

(a)

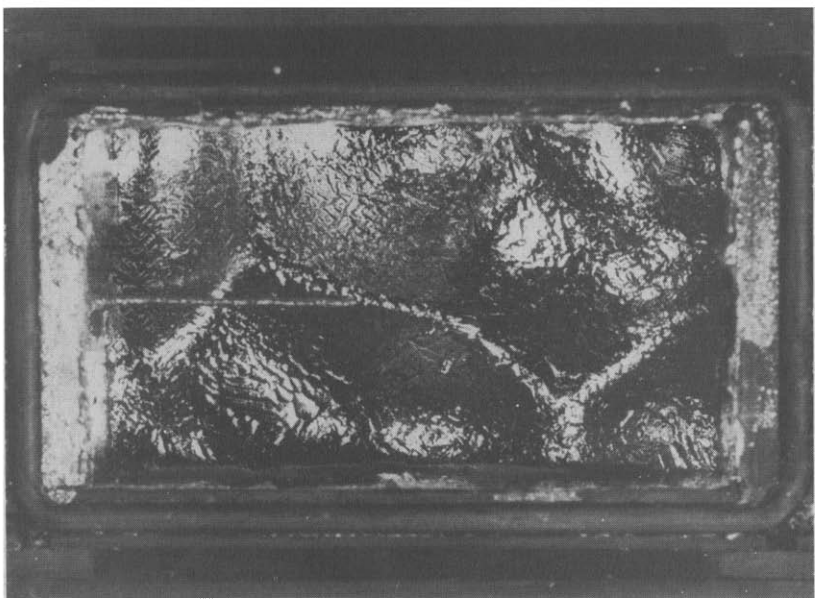

(b)

experiments. In some of the experiments a pair of circulation rolls with their axes perpendicular to the front and the back walls may have been formed. This is inferred from the semi-hollow shape of the interface (Fig. 7). The fluid rose near the two vertical sidewalls and fell near the central region of the test cell.

A sharp edge along the x-axis across the solid–liquid interface like a small ridge separating equally the front and the back portions was sometimes observed when a single or a pair of circulation rolls were formed in the melt. This suggests a secondary fluid motion which flows inward along the interface from the front and the back walls to the central region.

During melting from above the solid–liquid interface was smooth and flat, and the measured interface positions agreed with predictions of the Neumann model [15]. These findings provide further evidence that the anisotropy in the thermal conductivity of the liquid and of the crystal do not play an important role in controlling the heat transfer and the macroscopic interface shape during melting. The interface shape is primarily controlled by macroscopic natural convection in the melt.

Temperature distributions. Typical vertical temperature distributions at some preselected times during melting from below are shown in Fig. 10. In the early stages of the process, the Bénard convection did

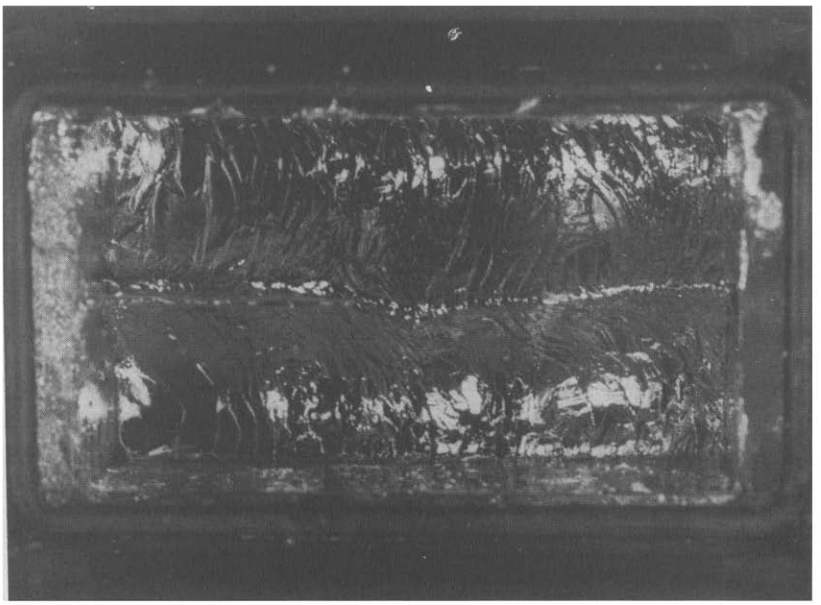

(c)

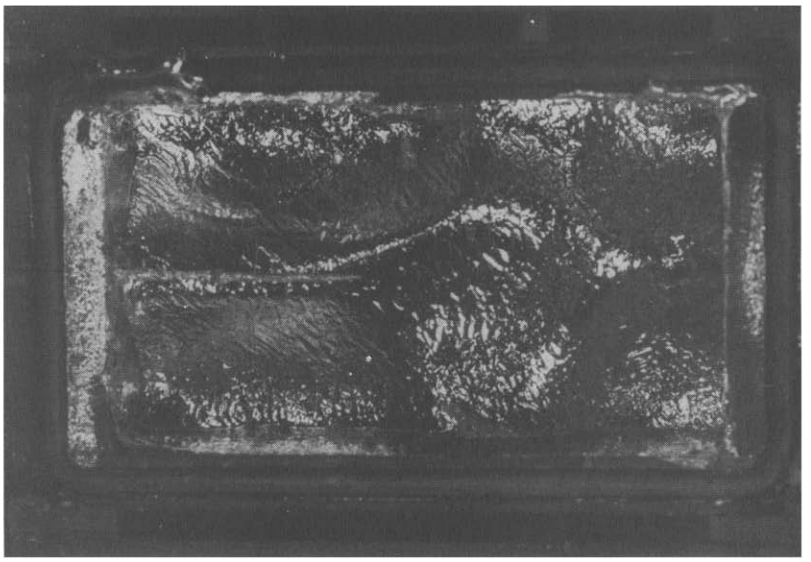

(d)

FIG. 8. Bénard capped cell distribution along the interface for $T_{wb} = 46.0°C$: (a) $t = 2$ min, (b) $t = 3$ min, (c) $t = 4$ min and (d) cylindrical capped roll appeared at $t = 3$ min.

produce a nonlinear temperature distribution in the liquid. The temperature gradient near the solid–liquid interface and at the bottom plate were steeper than near the central region of melt layer. The temperature distribution shown in the figure exhibits a very interesting feature. After natural convection has been established in the melt layer ($t \geqslant 8$ min), the vertical temperature gradients in the melt near the bottom of the test cell and below the interface appear to be adiabatic without being insulated.

At certain times the temperatures in the central core were significantly increased. The drastic difference in the temperature distribution suggests a complete change of the flow structure in the melt layer from one instant of time to the next. Turbulent natural convection was believed to be initiated. This caused a significant increase of energy transport from the bottom plate to the central core region and to the solid–liquid interface. However, the temperature distributions suggest that in spite of the high conductivity of the liquid metal the buoyancy induced turbulent motion of the fluid is so intense that most of the thermal energy near the bottom plate is advected to the upper region of the turbulent core where the temperatures are

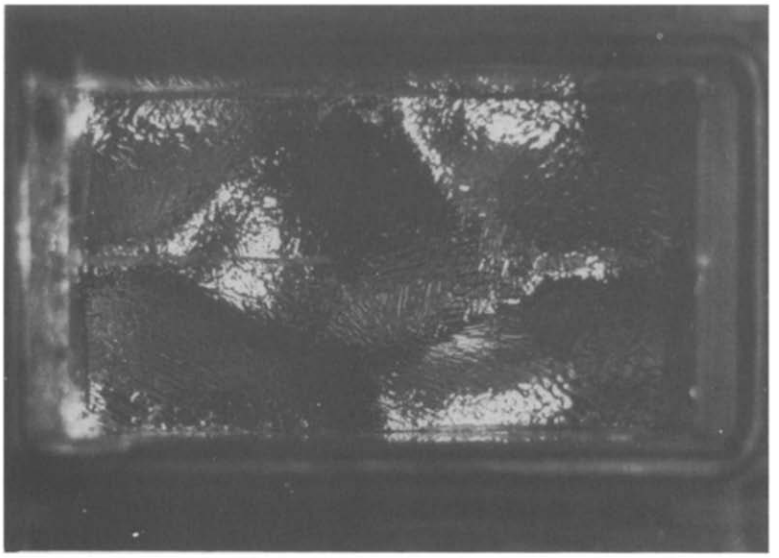

(a)

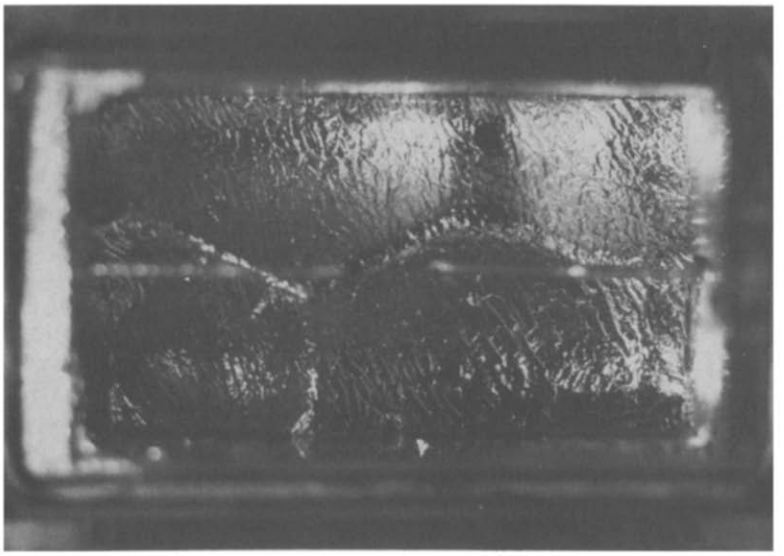

(b)

higher than near the lower region. This is in an opposite direction to the temperature gradient imposed by the heat source and sink. The peculiar phenomenon was not observed during melting of a paraffin (*n*-octadecane) which has relatively high Prandtl number [14]. The temperatures in the central core region decreased as melting proceeded but the reversal of the temperature gradient was not affected. This suggests that the flow structure did not change thereafter.

The findings concerning the temperature gradient reversal are consistent with published results for steady-state, turbulent natural convection in a fluid layer heated from below [17], except that in a liquid metal the gradients are much larger and do not disappear as the Rayleigh number is increased [15]. The gradient reversal is attributed to the dissipation of the thermals before reaching the upper boundary (solid–liquid interface). With increasing melt layer thickness (i.e. Rayleigh number) the temperature profile shows progressively gradual temperature variation from the bounding surfaces; however, the temperature gradient does not disappear.

The temperature gradient near the solid–liquid interface may decrease at a later time and does not appear to be as sharp as near the bottom plate. This may be due to the secondary flow along the interface in the z-direction, which drives the fluid back to the turbulent core near the central region. The flow decreased heat transport from the core to the interface and reduced the temperature gradient.

Temperature fluctuations. Figure 11(a) shows the temperature fluctuations recorded by the thermocouple located at 4.76 mm above the bottom plate. Initially, the temperature did not show any oscillations except for a linear rise after the interface passed over the

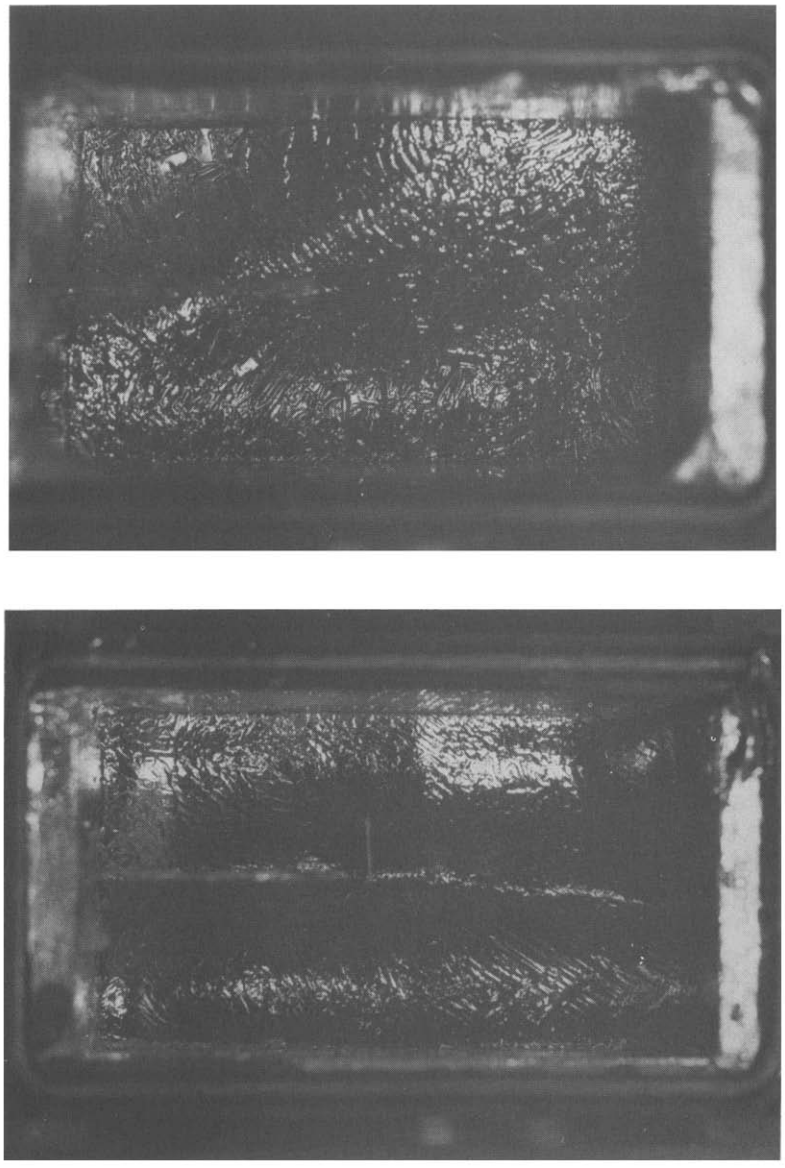

FIG. 9. Different convection modes can be inferred from the interface shape for $T_{wb} = 52.0°C$: (a) smaller size and larger number of Bénard cells at $t = 1.333$ min, (b) growth of Bénard cells at $t = 1.5$ min, (c) convection roll at $t = 1.833$ min, and (d) two modes of convection coexist in the melt.

thermocouple. Heat conduction is the only mode of heat transfer, and natural convection was not initiated. After several cycles of large amplitude temperature oscillations, the average temperature decreased suddenly and small amplitude, higher frequency temperature fluctuations appeared. The initial large amplitude temperature oscillations indicate: (1) the initiation of natural convection with the upper cooled fluid falling downward and the lower heated fluid rising upward, and (2) the gradual formation of Bénard convection cells or convection rolls. The small amplitude temperature fluctuations may be due to the growth and combination process of Bénard convection cells and/or the growth of the convection rolls. After a critical melt layer thickness has been exceeded, large amplitude and high frequency temperature fluctuations appeared (at $t = 3.25$ min, in Fig. 11a). This may indicate the breaking down of Bénard cells (convection rolls) and the laminar flow becoming random (turbulent). The upward moving fluid parcel near the bottom plate, passing over the sensor, caused a sharp increase in temperature. However, the increase in the mean temperature did not occur when a pair of circulation rolls were finally initiated. The downward flow near the central region passing over the sensor caused only large amplitude temperature fluctuations instead of having a sharp increase in the mean temperature [15].

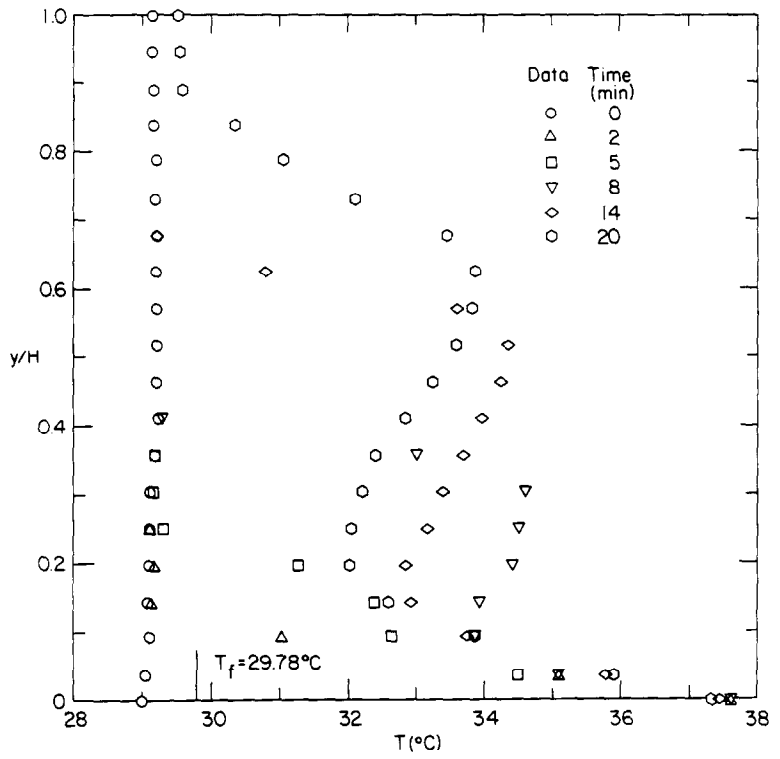

FIG. 10. Vertical temperature distributions at the central region during melting from below, $T_{wb} = 37.4°C$.

The flow in the melt layer was already turbulent when the solid–liquid interface passed over the thermocouple located at 24 mm above the bottom plate. The sharp increase in the mean temperature as well as the large amplitude and high frequency of fluctuations (around $t = 3.5$ min, in Fig. 11b) can be observed when recirculating flow was initiated. When the thermocouple was near the central core due to the advance of the interface, the amplitude and the frequency of temperature fluctuations decreased significantly, and the fluctuations became steady after the flow circulation became steady. This is due to the relatively small velocity of the fluid near the central region. An established circulation in the fluid should produce steady temperature fluctuations both near the bottom plate and the central region of the liquid layer. An unsteady or irregular flow structure resulting in an irregular interface shape may appear during the transition period and in some experiments may have persisted for some time. This can be inferred from the unsteady temperature fluctuation periods at both of the thermocouple locations.

For a smaller bottom temperature ($T_{wb} = 37.4°C$) the average temperature showed only a relatively small and gradual increase after the interface had passed over the sensor when a pair of circulation rolls were initiated [15]. The amplitude and frequency of the temperature fluctuations gradually increased. Significant temperature spikes were observed at later times because of the downward flowing parcels of fluid. It was found in different experiments that one of the circulation rolls may sometimes grow and the other shrink. When this occurs, the growing roll may merge with the shrinking one and a unicellular circulation would be established at later times. This can be inferred from the temperature fluctuation measurements [15]. Only a small increase in a mean temperature due to the cool downward flowing parcels of the two rolls was observed initially. Large amplitude temperature fluctuations appeared later, decreased gradually and became small in the final stage of the melting process.

Melting rate. The melted volume was measured at different times and the results are plotted in Fig. 12. The fraction of melted volume increases almost linearly with the dimensionless time except at the very early stages of the melting process and has the same trend as predicted by the one-dimensional model. The melting rate as indicated by data points increases with the Stefan number. Although the measured melting rates are higher than the predicted ones based on the one-dimensional model, the agreement is reasonably good. This may be explained by the fact that during the experiments the nonplanar interface shape results in a larger contact area between the solid and the liquid phases and thus increases the melting rate. In addition, the model uses the average, steady-state heat transfer coefficient for natural convection in the absence of phase change [11], and this may contribute to the discrepancy between the data and predictions.

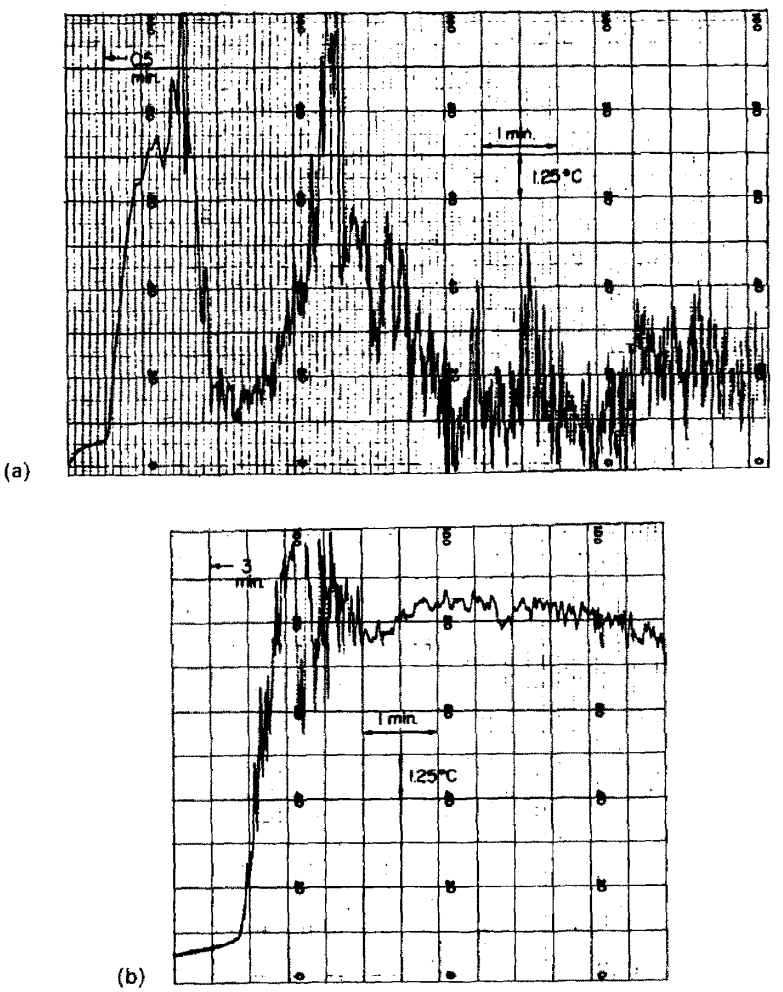

FIG. 11. Temperature fluctuations during melting from below for $T_{wb} = 46.0°C$ with unicellular circulation formed in the melt: (a) the thermocouple located at 4.76 mm above the bottom plate, and (b) thermocouple located 24 mm above the bottom plate.

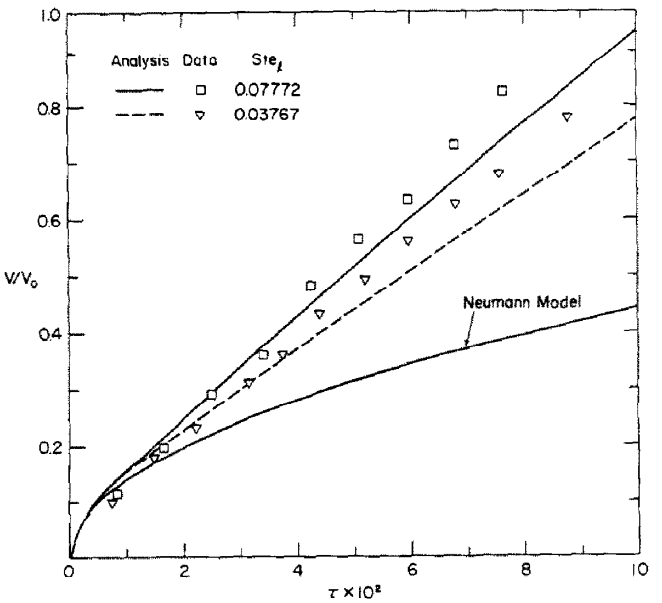

FIG. 12. Comparison of the measured and predicted melted volume fractions.

However, most of the melting occurs in the turbulent regime irrespective what flow structure was formed. As predicted, turbulent natural convection in the liquid can significantly increase the melting rate.

Even though the upper test cell wall is not truly adiabatic, the measured melting rates are nearly constant. This finding suggests that the average Nusselt number across the melt layer is proportional to the 1/3 power of the Rayleigh number if both dimensionless parameters are based on the average height of the liquid layer. This result is very similar to that of natural convection heat transfer in a rectangular enclosure for turbulent flow [11]. However, the instantaneous local heat transfer coefficient at the solid–liquid interface, which can be approximated by

$$h \approx \frac{\rho_s \Delta h_f}{(T_{wb} - T_f)} \frac{ds}{dt}, \tag{12}$$

is expected to show significant variation both with location and time. This may be inferred from the timewise variation of the solid–liquid interface positions given in Fig. 7.

5. CONCLUSIONS

The effect of natural convection on solid–liquid phase-change heat transfer under gravitationally unstable situations (i.e. melting from below and solidification from above) have been studied experimentally. Use of a pure metal (gallium) allowed also examination of the crystallographic effects on the solid–liquid interface morphology. Based on the results obtained the conclusions of the study are as follows:

During the solidification of gallium from above, the anisotropy in the thermal conductivity and the interface growth morphology always play an important role in controlling the interface shape. The presence of natural convection in the liquid slows down the rate of solidification and further complicates the transport processes and the interface morphology.

During the melting of gallium from below, the anisotropy in the thermal conductivity and interface morphology are not as important as during solidification, and heat transfer controls the interface shape and motion. Bénard convection cells or convection rolls appeared initially and grew in size as the melting progressed. The transition from laminar to turbulent ('mixed') flow was evident from the large increase in temperature of the melt and a sharp increase in amplitude and frequency of temperature fluctuations. The intense circulation in the test cell caused a reversal of temperature gradient in the liquid core. Natural convection in the liquid was found to significantly distort the solid–liquid interface and increase the melting rate.

The average position of the phase change boundary was predicted reasonably well from a simple one-dimensional model which ignored anisotropy of the gallium crystals but accounted for natural convection heat transfer at the solid–liquid interface.

The test cell used in the experiments was small; therefore, the results reported may to some extent be geometry specific. The flow in the melt was three-dimensional, time-dependent and was affected by the microscopic morphology and the macroscopic contour of the interface. As a result, the flow structure and the macroscopic solid–liquid interface positions were not reproducible. Experiments need to be performed in a much larger test cell in order to establish the importance of the test cell sidewalls and of the three-dimensional flow effects during phase-change of a pure metal under unstable conditions.

Acknowledgements—The work described in this paper was supported by the National Science Foundation Heat Transfer Program under grant Nos. MEA-8104061 and MEA-8313573.

REFERENCES

1. A. W. D. Hills, S. L. Malhotra and M. R. Moore, The solidification of pure metals (and eutectics) under unidirectional heat flow condition: II. Solidification in the presence of superheat, *Met. Trans.* **6B**, 131–142 (1975).
2. F. M. Chiesa and R. I. L. Guthie, Natural convective heat transfer rates during the solidification and melting of metals and alloy systems, *J. Heat Transfer* **96**, 377–384 (1974).
3. W. C. Winegard and G. S. Cole, Thermal convection during horizontal solidification of pure metals and alloys, *J. Inst. Metals* **93**, 153–164 (1964).
4. G. S. Cole and G. F. Bolling, The importance of natural convection in casting, *Trans. metall. Soc. A.I.M.E.* **233**, 1568–1572 (1965).
5. K. Morizane, A. F. Witt and H. C. Gatos, Impurity distribution in single crystals, *J. electrochem. Soc.* **114**, 738–742 (1967).
6. J. Szekely and P. S. Chhabra, The effect of natural convection on the shape and movement of the melt-solid interface in the controlled solidification, *Met. Trans.* **1B**, 1195–1203 (1970).
7. K. M. Fisher, The effects of fluid flow on solidification of industrial castings and ingots, *PhysicoChem. Hydrodynam.* **2**, 311–326 (1981).
8. C. Gau and R. Viskanta, Melting and solidification of a metal system in a rectangular cavity. *Int. J. Heat Mass Transfer* **27**, 113–123 (1984).
9. M. Flemings, *Solidification Processing*. McGraw-Hill, New York (1974).
10. W. H. Cubberly, *Metal Handbook, Properties and Selection: Nonferrous Alloys and Pure Metals* (9th edn.), pp. 736–737. American Society of Metals, Metals Park, Ohio (1979).
11. K. G. T. Hollands and G. D. Raithby, Natural convection, in *Handbook of Heat Transfer* (2nd edn.) (edited by W. M. Rohsenow, J. P. Hartnett and E. N. Ganic). McGraw-Hill, New York (1985).
12. K. A. Jackson, Interface structure, in *Growth and Perfection of Crystals* (edited by R. H. Doremus, B. W. Roberts and D. Turnbull), pp. 319–324. John Wiley, New York (1958).
13. G. A. Alfintsev and D. E. Ovsienko, Growth mechanism of gallium crystals grown from melts, *Soviet Phys. Dokl.* **9**, 489–491 (1964).
14. R. Viskanta, C. J. Ho and C. Gau, Phase-change heat transfer in rectangular cavity, in *Multi-Phase Flow and Heat Transfer III. Part B: Applications* (edited by T. N.

Veziroglu and A. E. Bergles), pp. 541–563. Elsevier Science Publishers, Amsterdam (1984).
15. C. Gau, Heat transfer during solid–liquid phase transformation of metals in rectangular cavities, Ph.D. Thesis, Purdue University, W. Lafayette, Indiana (1984).
16. H. Oertel Jr., Three-dimensional convection within rectangular boxes, in *Natural Convection in Enclosures* (edited by K. E. Torrance and I. Catton), pp. 11–16. ASME, New York (1980).
17. T. Y. Chu and R. J. Goldstein, Turbulent convection in a horizontal layer of water, *J. Fluid Mech.* **60**, 141–159 (1973).

EFFET DE LA CONVECTION NATURELLE SUR LA SOLIDIFICATION PAR DESSUS ET LA FUSION PAR DESSOUS D'UN METAL PUR

Résumé—On étudie le rôle de la convection naturelle sur le mouvement de l'interface solide–liquide pendant la fusion par dessus et la solidification par dessous d'un métal pur. Les mesures des distributions et des fluctuations de température sont utilisées comme indication qualitative des régimes de convection naturelle et des structures de fusion pendant le changement de phase. Les photographies de la morphologie de l'interface après drainage du liquide hors de la cellule révèlent une structure compliquée d'écoulement en fonction du temps dans le liquide. Les positions mesurées (moyennes) et calculées de l'interface solide–liquide pendant l'opération montrent une correspondance relativement bonne.

EINFLUSS DER NATÜRLICHEN KONVEKTION AUF DAS ERSTARREN EINES REINEN METALLS VON OBEN UND DAS SCHMELZEN VON UNTEN

Zusammenfassung—Die Rolle der natürlichen Konvektion bei der Bewegung der Phasengrenze während des Schmelzens eines reinen Metalls von unten und des Erstarrens von oben wurde untersucht. Die Messungen der Temperaturverteilungen und -schwankungen wurden als qualitative Anzeigen der Gebiete mit natürlicher Konvektion und der Struktur der Schmelze während der Phasenumwandlung verwendet. Fotos von der fest-flüssigen Grenzflächenmorphologie (nach Ablassen der Schmelze aus der Testzelle) enthüllten eine komplizierte zeitabhängige Strömungsstruktur in der Flüssigkeit. Die gemessene (durchschnittliche) und die berechnete Position der Phasengrenze während des Erstarrens von oben und Schmelzens von unten zeigen eine verhältnismäßig gute Übereinstimmung.

ВЛИЯНИЕ ЕСТЕСТВЕННОЙ КОНВЕКЦИИ НА ЗАТВЕРДЕВАНИЕ СВЕРХУ И ПЛАВЛЕНИЕ СНИЗУ ЧИСТОГО МЕТАЛЛА

Аннотация—Изучена роль естественной конвекции на движение границы раздела твердое тело–жидкость при плавлении снизу и затвердевании сверху чистого металла. Для получения качественной характеристики режимов свободно-конвективного течения и структур плавления при фазовых превращениях измерялись как распределение, так и флуктуации температуры. Фотографии морфологии границы раздела твердое теложидкость (после удаления расплава из исследуемой ячейки) показали сложную, зависящую от времени структуру течения в жидкости. Измеренные (средние) и рассчитанные положения границы раздела твердое тело–жидкость при затвердевании сверху и плавлении снизу дали довольно хорошее совпадение.